Convection in two-layer systems with an anomalous thermocapillary effect

L. M. Braverman,[1] K. Eckert,[2] A. A. Nepomnyashchy,[3,4] I. B. Simanovskii,[3] and A. Thess[2]
[1]*Department of Computer Science, Carmiel ORT College, Carmiel, Israel*
[2]*Center for Physical Fluid Dynamics, Department of Mechanical Engineering, Dresden University of Technology, 01062 Dresden, Germany*
[3]*Department of Mathematics, Technion-Israel Institute of Technology, 32000 Haifa, Israel*
[4]*Minerva Centre for Nonlinear Physics of Complex Systems, Technion-Israel Institute of Technology, 32000 Haifa, Israel*
(Received 18 March 1999; revised manuscript received 5 March 2000)

Recently, it was found that the anomalous thermocapillary effect (the interfacial tension increases with temperature) is typical for various liquid-liquid systems. We consider the combined action of buoyancy and thermocapillary instability mechanisms in systems with an anomalous thermocapillary effect on the interface. The problem is solved in both linear and nonlinear formulations. A special type of oscillatory instability has been found and investigated.

PACS number(s): 47.27.−i

I. INTRODUCTION

The phenomenon of Rayleigh–Bénard convection in a horizontal layer between rigid boundaries, which is a paradigmatic example of the pattern formation in nonequilibrium systems, has been studied extensively during the last decades [1,2]. The convection phenomena in the presence of *an interface* are still less investigated.

Two main instability mechanisms exist in systems with an interface. The *buoyancy* instability mechanism (caused by a *volume* effect) is more important for relatively thick layers, while the *thermocapillarity* (an *interfacial* effect) plays the dominant role in the case of thin layers or under microgravity conditions. Many works are devoted to the limit cases of ''pure'' buoyancy-driven (Rayleigh–Bénard) convection and ''pure'' thermocapillarity-driven (Marangoni–Bénard) convection. For the Rayleigh–Bénard convection in systems with an interface both stationary [3] and oscillatory [4–7] instabilities are possible; for a review, see Ref. [8]. Several phenomena, which include cellular pattern formation [9–13], deformational instability leading to the appearance of a dry spot [14,15,13], longitudinal [16–19] and transverse [20,21], oscillatory instabilities, have been discovered in the case of the Marangoni–Bénard convection.

Novel effects are expected to arise from the combined action of buoyancy and thermocapillary forces. There are only a few works where the combined action of both instability mechanisms is investigated. The case where both instability mechanisms produce forces acting in the same direction, is better explored. Such a situation takes place, e.g., for the stationary convection in a liquid layer with the free upper surface in the case of the normal thermocapillary effect (when the surface tension decreases with temperature). The corresponding linear stability theory was developed by Nield [22] in the framework of a one-layer approach, and later it was extended to the case of liquid–liquid two-layer systems by Refs. [23,24]. The nonlinear development of instability was studied theoretically in Refs. [25,26] and experimentally in Refs. [23,24,27,28].

There is another possibility: both effects produce forces acting in opposite directions. In the case of the normal thermocapillary effect, this situation takes place in a two-layer system if the buoyancy convection is generated mainly in the upper layer [29]. The interfacial temperature distribution produced by the buoyancy convection generates tangential stresses which brake the fluid motion. In this case, the stationary instability threshold increases. Moreover, in the case where the characteristic time scales of heat transfer and momentum transfer differ essentially, the competition between two mechanisms of stationary instability can produce oscillations [8,29].

In this paper we investigate the interaction between buoyancy and thermocapillary instability mechanisms in a two-layer system in the case of an *anomalous* thermocapillary effect (the interfacial tension increases with temperature). It was observed in aqueous alcohol solutions, nematic liquid crystals, binary metallic alloys, etc. (see, e.g., Ref. [30] and references therein). There are indications that the occurrence of an anomalous thermocapillary effect might be a typical property of various liquid–liquid systems [31]. That is why the realistic models of multilayer convection should take into account the possibility of the anomalous thermocapillary effect.

To our knowledge, until now the investigation of convection in a two-layer system with anomalous thermocapillary effect was done only in the series of papers [32–34]. In those papers, the attention was paid to the buoyancy-driven convection in the presence of the thermocapillary effect, interface viscosity, and interface deformation. It was found that the anomalous thermocapillary effect could essentially enhance the width of the interval of the oscillatory instability.

Here we demonstrate that the anomalous thermocapillary effect can lead to a new kind of the oscillatory instability caused by the competition between the buoyancy force and the thermocapillary tangential stresses. This kind of the oscillatory instability sets in when the buoyancy convection is generated mainly in the lower layer.

The paper is organized as follows. After formulating the problem in Sec. II we analyze the linear stability of the system in Sec. III. The special features of the particular convective regimes are studied by means of two-dimensional numerical simulations in Sec. IV. To be close to real systems,

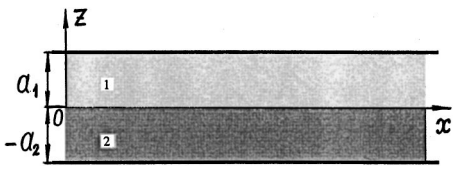

FIG. 1. Geometrical configuration of the region and coordinate axes.

the majority of calculations are done for the two-layer system 10 cS silicone oil over ethylenglycol which reveals the anomalous thermocapillary effect.

II. FORMULATION OF THE PROBLEM

We consider a system of two horizontal layers of immiscible fluids with different physical properties (see Fig. 1). The system is bounded from above and from below by two isothermic rigid plates kept at constant different temperatures (the total temperature drop is Θ; the heating is from below). It is assumed that the interfacial tension σ *grows* linearly with the temperature: $\sigma=\sigma_0-\alpha T$, where $\alpha<0$. We disregard the deformation of the interface, because it can essentially influence the convective instability only in the case of extremely thin layers [15] or in the case of a small density difference between fluids [33], [34]. These cases are not considered in this paper. The variables referring to the upper layer are marked by index 1, the variables referring to the lower layer are marked by index 2.

Density, kinematic and dynamic viscosity, heat conductivity, thermal diffusivity, heat expansion coefficient of the mth fluid are, respectively, ρ_m, ν_m, η_m, κ_m, χ_m, and β_m; a_m is the thickness of the mth layer ($m=1,2$). Let us introduce the following notations:

$$\rho=\rho_1/\rho_2, \quad \nu=\nu_1/\nu_2, \quad \eta=\eta_1/\eta_2, \quad \kappa=\kappa_1/\kappa_2,$$

$$\chi=\chi_1/\chi_2, \quad \beta=\beta_1/\beta_2, \quad a=a_2/a_1.$$

As the units of length, time, velocity, pressure, and temperature we use a_1, a_1^2/ν_1, ν_1/a_1, $\rho_1\nu_1^2/a_1^2$, and Θ.

The investigation of the convection were performed for the 10 cS silicone oil–ethylenglycol real system. The physical parameters are summarized in Table I. The measurement of the temperature dependence of interfacial tension, done by the LAUDA AG (Germany), showed the existence of an anomalous thermocapillary effect: $\alpha=-0.0127$ mN/m K. A more detailed study of this effect is in preparation [31]. The ratios of parameters of two fluids are: $\rho=0.846$, $\nu=0.6493$, $\eta=0.549$, $\kappa=0.6194$, $\chi=1.096$, $\beta=1.4516$; the Prandtl number $P=94$.

The complete nonlinear equations of convection in frames of the Boussinesq approximation [8] for both fluids have the following form:

$$\frac{\partial \mathbf{v}_1}{\partial t}+(\mathbf{v}_1\cdot\boldsymbol{\nabla})\mathbf{v}_1=-\boldsymbol{\nabla}p_1+\nabla^2\mathbf{v}_1+GT_1\boldsymbol{\gamma},$$

$$\frac{\partial T_1}{\partial t}+\mathbf{v}_1\cdot\boldsymbol{\nabla}T_1=\frac{1}{P}\nabla^2T_1, \tag{1}$$

$$\boldsymbol{\nabla}\cdot\mathbf{v}_1=0;$$

$$\frac{\partial \mathbf{v}_2}{\partial t}+(\mathbf{v}_2\cdot\boldsymbol{\nabla})\mathbf{v}_2=-\rho\boldsymbol{\nabla}p_2+\frac{1}{\nu}\nabla^2\mathbf{v}_2+\frac{G}{\beta}T_2\boldsymbol{\gamma},$$

$$\frac{\partial T_2}{\partial t}+\mathbf{v}_2\cdot\boldsymbol{\nabla}T_2=\frac{1}{\chi P}\nabla^2T_2, \tag{2}$$

$$\boldsymbol{\nabla}\cdot\mathbf{v}_2=0.$$

Here $G=g\beta_1\Theta a_1^3/\nu_1^2$ is the Grashof number (g is the gravity acceleration), $P=\nu_1/\chi_1$ is the Prandtl number, $\boldsymbol{\gamma}$ is the unit vector directed vertically upward. The conditions on the isothermic rigid boundaries are:

$$\mathbf{v}_1=\mathbf{0}, \quad T_1=0, \quad z=1, \tag{3}$$

$$\mathbf{v}_2=\mathbf{0}, \quad T_2=1, \quad z=-a. \tag{4}$$

The boundary conditions on the interface $z=0$ include conditions for the tangential stresses:

$$\eta\frac{\partial v_{1x}}{\partial z}-\frac{\partial v_{2x}}{\partial z}-\frac{\eta M}{P}\frac{\partial T_1}{\partial x}=0, \tag{5}$$

$$\eta\frac{\partial v_{1y}}{\partial z}-\frac{\partial v_{2y}}{\partial z}-\frac{\eta M}{P}\frac{\partial T_1}{\partial y}=0, \tag{6}$$

$$z=0$$

the continuity of the velocity field:

$$\mathbf{v}_1=\mathbf{v}_2, \quad z=0, \tag{7}$$

the continuity of the temperature field:

$$T_1=T_2, \quad z=0, \tag{8}$$

and the continuity of the heat flux normal components:

$$\kappa\frac{\partial T_1}{\partial z}-\frac{\partial T_2}{\partial z}=0, \quad z=0. \tag{9}$$

TABLE I. Material properties of the silicone oil–ethylenglycol system.

	ρ_i (k g m^{-3})	ν_i (10^{-4} m^2 s^{-1})	κ_i (W m^{-1} K^{-1})	χ_i (10^{-4} m^2 s^{-1})	β_i (K^{-1})
Silicone oil ($i=1$)	940.0	0.10	0.16	0.00106	0.0009
Ethylenglycol ($i=2$)	1110.0	0.154	0.258	0.00097	0.0006

Here $M=\alpha\Theta a_1/\eta_1\chi_1$ is the Marangoni number, which is negative by definition in the case of an anomalous thermocapillary effect.

The problem (1)–(9) for any choice of parameters has the solution

$$\mathbf{v}_1^0=\mathbf{v}_2^0=\mathbf{0},$$

$$T_1^0=-\frac{z-1}{1+\kappa a},\quad T_2^0=-\frac{\kappa z-1}{1+\kappa a},$$

$$p_1^0=-\frac{G}{1+\kappa a}\left(\frac{z^2}{2}-z\right), \tag{10}$$

$$p_2^0=-\frac{G}{\rho\beta(1+\kappa a)}\left(\frac{\kappa z^2}{2}-z\right),$$

corresponding to mechanical equilibrium. In the following sections we shall investigate its instability and the regimes of convection which appear due to this instability.

III. LINEAR STABILITY THEORY

A. Description of the method

The stability of the mechanical equilibrium can be investigated in frames of the linear stability theory. The boundary value problem (1)–(9) is linearized around the solution (10). The solutions of the linearized problem are presented as a superposition of normal modes characterized by a wave vector $\mathbf{k}=(k_x,k_y)$ and a complex growth rate $\lambda=\lambda_r+i\lambda_i$:

$$[\tilde{\mathbf{v}}_1(z),\tilde{p}_1(z),\tilde{T}_1(z),\tilde{\mathbf{v}}_2(z),\tilde{p}_2(z),\tilde{T}_2(z)]\times\exp(ik_xx+ik_yy+\lambda t); \tag{11}$$

where subsequently the sign ''tilde'' will be omitted.

Since the problem is isotropic, the growth rate λ depends only on the wave vector modulus $k=|\mathbf{k}|$ but not on its direction. That is why it is sufficient to consider only two-dimensional disturbances with $\mathbf{k}=(k,0)$ which do not depend on the coordinate y. Introducing the stream function disturbances

$$v_{mx}=\psi_m',\quad v_{mz}=-ik\psi_m(m=1,2),$$

where the prime stands for d/dz, and eliminating pressure disturbances in the usual way, we obtain the following boundary eigenvalue problem:

$$-\lambda D\psi_m=-c_mD^2\psi_m+ikGb_mT_m, \tag{12}$$

$$\lambda T_m-ikA_m\psi_m=\frac{d_m}{P}DT_m,\quad (m=1,2), \tag{13}$$

$$\psi_1=\psi_1'=T_1=0,\quad z=1, \tag{14}$$

$$\psi_2=\psi_2'=T_2=0,\quad z=-a, \tag{15}$$

$$\eta\psi_1''-\psi_2''-\frac{ik\eta M}{P}T_1=0,\quad z=0, \tag{16}$$

$$\psi_1'=\psi_2', \tag{17}$$

$$\psi_1=\psi_2=0, \tag{18}$$

$$T_1=T_2, \tag{19}$$

$$\kappa T_1'=T_2', \tag{20}$$

where $c_1=b_1=d_1=e_1=1$, $c_2=1/\nu$, $b_2=1/\beta$, $d_2=1/\chi$, $e_2=\rho$; $A_1=dT_1^0/dz=-1/(1+\kappa a)$, $A_2=dT_2^0/dz=-\kappa/(1+\kappa a)$ are the dimensionless temperature gradients.

We found the linear stability boundaries by means of the following method. In the case of a stationary instability mode, we put $\lambda=0$ for fixed values of G and k. We construct three linearly independent solutions of Eqs. (12) and (13) in the upper fluid satisfying the boundary conditions (14), and three linearly independent solutions in the lower fluid satisfying the boundary conditions (15), by means of the standard Runge–Kutta–Merson method, and construct a linear combination of these solutions satisfying boundary conditions (17)–(20). Then we calculate the Marangoni number from the boundary condition (16). In the case of an oscillatory instability, we put $\lambda_r=0$ and take some trial λ_i. The Marangoni number obtained from Eq. (16) is generally complex: $M=M_r+iM_i$. Then frequency λ_i and the corresponding stability boundary $M=M_r$ is found from the relation

$$M_i(\lambda_i)=0$$

by means of iterations. Thus, we obtain the *neutral surfaces* $\lambda_r(M,G,k)=0$ in the form $M=M(G,k)$.

B. Stationary instability (layers with equal thicknesses)

Let us define the *local* Rayleigh numbers determined by parameters of each layer:

$$R_m=\frac{g\beta_mA_ma_m^4}{\nu_m\chi_m},\quad m=1,2.$$

Their ratio

$$\frac{R_2}{R_1}=\frac{\kappa\nu\chi a^4}{\beta},$$

can be used in order to estimate in which layer the buoyancy effects are stronger. We will consider the system with the physical parameters given in Table I. If we choose $a=1$, then $R_2/R_1=0.304$. Because $R_1>R_2$, we can expect that the buoyancy convection is generated mainly in the upper layer, while in the lower layer only a weak induced motion appears. In this case the temperature distribution on the interface formed by the buoyancy convection, generates the thermocapillary stresses which support the buoyancy convection (under the condition of the anomalous thermocapillary effect, i.e., $M<0$). In such a situation we can expect the appearance of the stationary instability and the absence of the oscillatory one.

Let us describe the results of calculations in the case $a=1$. The typical cross sections of the neutral surfaces $\lambda_r(G,M,k)$ for fixed values of G are presented in Fig. 2. Solid lines correspond to boundaries of stationary instability,

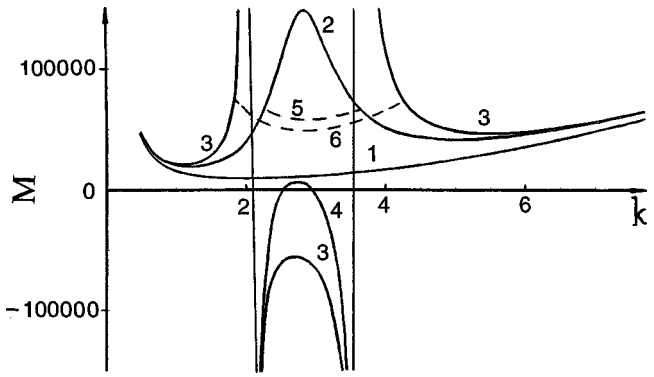

FIG. 2. Neutral curves in the case $a=1$: $G=0$ (line 1), $G=5$ (lines 2, 5), $G=6$ (lines 3, 6), $G=24$ (line 4).

dashed lines correspond to boundaries of oscillatory instability. If $G=0$, the stationary instability would be realized only in the case of *normal* thermocapillary effect ($M>0$, see line 1). When G grows, a local maximum appears on the stationary stability curve (see line 2). For a certain value of G the maximum tends to infinity, and the stationary stability curve is split into three fragments (see line 3). Only one of these fragments is located in the physical region $M<0$ and describes some stationary instability in the case of *anomalous* thermocapillary effect. At $G=22.6$ this ''physical'' fragment of the stability curve touches the axis $M=0$. That means that for this value of the Grashof number the buoyancy convection would appear in the system in the absence of the thermocapillary effect. For larger values of G this fragment crosses the axis $M=0$ (see line 4). The boundaries of oscillatory instability (lines 5, 6) are located in the region $M>0$ which is physically irrelevant.

The stability region obtained by minimization of the neutral curves with respect to k is shown in Fig. 3 (lines 1, 2). Let us emphasize that in real experiments the geometric parameters of the system are fixed, while the temperature drop is changed, so that the Marangoni number M and the Grashof number G are proportional, and their ratio

$$K=\frac{|M|}{G}=\frac{|\alpha|P}{g\beta_1\rho_1 a_1^2}$$

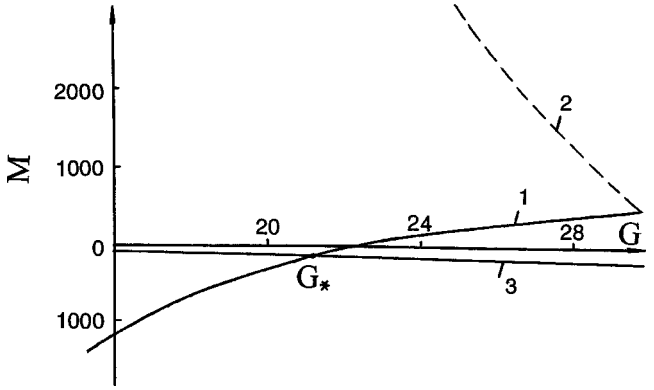

FIG. 3. Stability region in the case $a=1$: stationary stability boundary (line 1); oscillatory stability boundary (line 2); straight line corresponding to $K=5.75$.

is constant, e.g., in the case of the two-layer system with $a=1$ and the total thickness $a_1+a_2=1$ cm we find $K=5.75$ (see line 3 of Fig. 3). In the latter case, using the results shown in Fig. 3 we can predict that the convection will start as $G=G_*=21.4$, $M=M_*=-123$ which corresponds to the total temperature drop $\Theta=1.94$ K.

C. Oscillatory instability (layers with unequal thicknesses)

Next we consider the case where the buoyancy convection first appears mainly in the lower layer. As an example, we present results obtained for the thickness ratio of $a=1.8$ corresponding to the Rayleigh numbers' ratio $R_2/R_1=3.19$. We now have the situation where the buoyancy convection first appears in the lower layer.

In order to understand the relations between buoyancy and thermocapillary effect in the given system, let us assume that there is a local positive temperature fluctuation (''hot spot'') on the interface. The buoyancy generates an upstream flow beneath the hot spot, and a divergent flow on the interface near the hot spot. At the same time, the anomalous thermocapillary effect produces thermocapillary stresses that tend to form a convergent flow on the interface near the hot spot and a downstream flow in the lower layer. Thus, thermocapillary stresses tend to suppress the buoyancy convection. The competition between the buoyancy and the thermocapillary effect leads to stabilization of the stationary instability. Moreover, the asynchronic action of the buoyancy and the thermocapillary effect may lead to the appearance of oscillatory instability.

In the next section we shall discuss the convective oscillations in more detail. Here we present the results of the linear stability theory. Some typical neutral curves are shown in Fig. 4(a). Corresponding dependencies of the frequency λ_i on the wave number k along the neutral curves are presented in Fig. 4(b). One can see that in the region $15<G<15.5$ the stationary neutral curves (solid lines) change rather slowly with G. As $G<G_1=15.1$, the oscillatory neutral curve is absent. At $G>G_1$, a closed region of oscillatory instability (dashed line) appears. It grows rapidly with G and at last touches the stationary neutral curve as $G=G_2=15.3$. The stability boundaries in the $(M-G)$-plane for the stationary and oscillatory instabilities are shown in Fig. 5. One can conclude that in the case $K=|M|/G<K_*=31.7$ only the stationary instability will be observed. Using the physical parameters of the system, we find that the latter case will take place if the total thickness of the two-layer system is larger than 5.9 mm. If the thickness of the two-layer system is smaller than the critical one, some slow oscillations appear near the threshold. The dependencies of the frequency $\omega=\lambda_i$ and of the wave number on the ratio K for the critical oscillatory mode are shown in Fig. 6. Let us note that the *dimensional* frequency $\Omega=\omega\nu_1/a_1^2$. For instance, in the case of the total thickness $a_1+a_2=4$ mm ($K=70.3$) we find $\Omega=0.21\ \mathrm{s}^{-1}$.

IV. 2D SIMULATIONS OF NONLINEAR CONVECTIVE REGIMES

The linear theory predicts the behavior of infinitesimally small disturbances in the infinite layers. Actually, the real

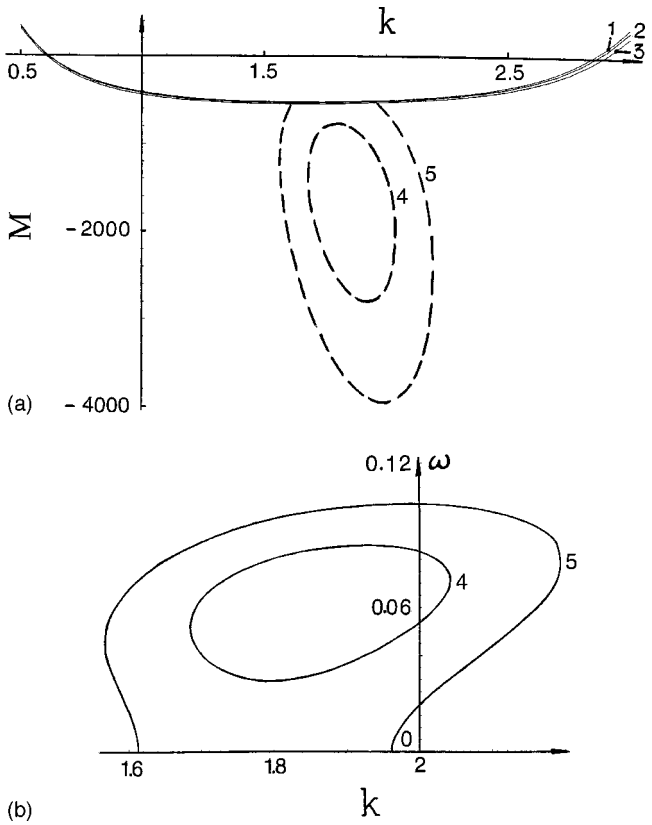

FIG. 4. (a) Neutral curves in the case $a=1.8$: $G=15$ (line 1), $G=15.2$ (lines 2, 4), $G=15.5$ (lines 3, 5). (b) Dependencies $\lambda_i(k)$: $G=15.2$ (line 4), $G=15.5$ (line 5).

system has rigid lateral boundaries. The influence of the lateral boundaries depends on the kind of instability. In the case of a stationary instability, which is always *absolute* (the disturbance grows in any spatial point) the influence of the lateral boundaries is restricted to a quantization of eigenmodes and to an additional viscous dissipation near the boundaries. As the result, the threshold Marangoni number, $|M|$, and Grashof number, G, are slightly enhanced compared with the case of an infinite layer. In the case of an oscillatory instability, the influence of the lateral boundaries can be much stronger, especially near the threshold where the oscillatory

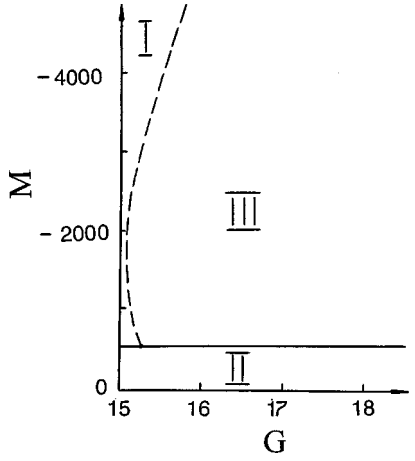

FIG. 5. Stability regions in the case $a=1.8$; I–stability, II–stationary instability; III–oscillatory instability.

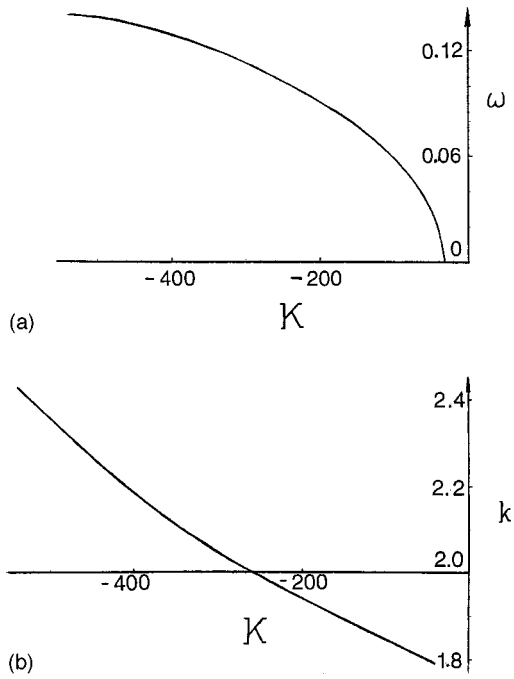

FIG. 6. Dependencies of (a) critical frequency $\omega=|\lambda_i|$ and (b) critical wave number k on the ratio K in the case $a=1.8$.

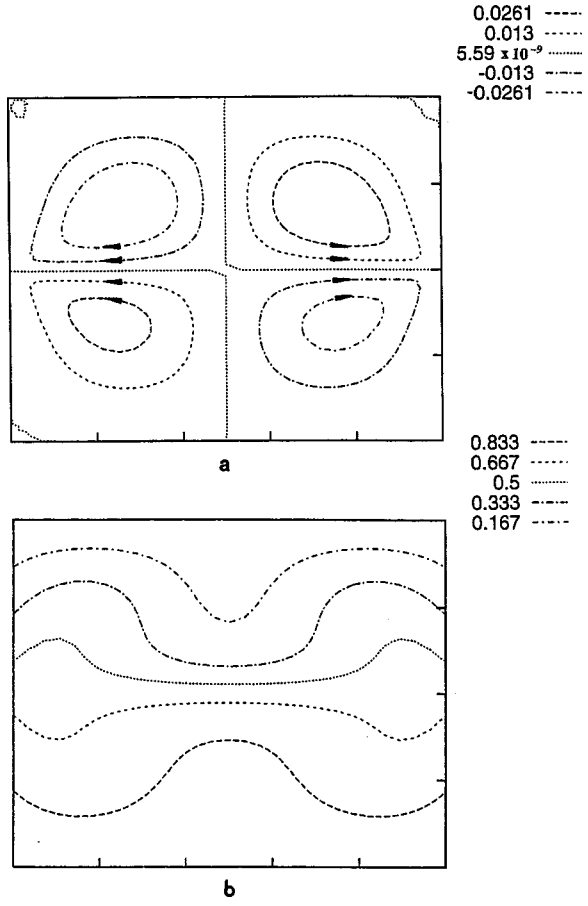

FIG. 7. Stationary convective motion driven mainly by thermocapillarity. (a) Streamlines and (b) isotherms. Parameters: $a=1$; $G=25$, $M=-4.275\times10^4$.

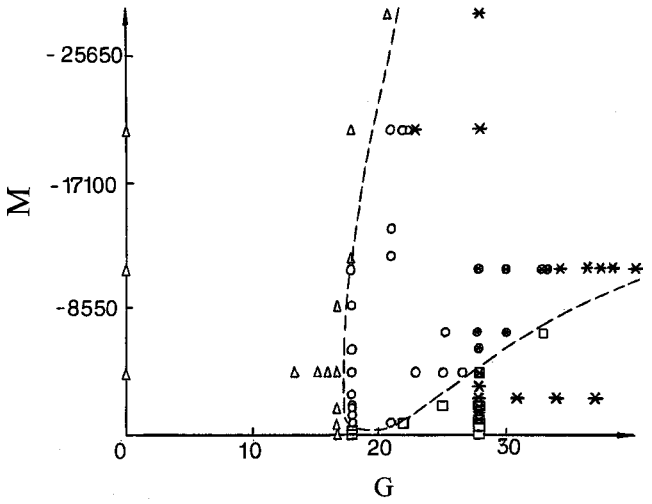

FIG. 8. The diagram of different regimes in the plane (G, $-M$). Triangles–mechanical equilibrium, squares–stationary state, circles–symmetric oscillations, stars–asymmetric oscillations.

instability is *convective*. In the latter case, small disturbances in the infinite layers grow only in the moving reference frame but decay in any fixed spatial point. In the finite region, some steady wavy patterns can appear in the region of a convective instability, only if the reflection of waves on the lateral boundaries is strong enough. Generally, one can expect that the shift of the critical Marangoni and Grashof numbers is more essential in the case of the oscillatory instability than in the case of the stationary instability.

In order to analyze the influence of the lateral boundaries, we perform nonlinear simulations of convection in a closed cavity. Another reason for nonlinear simulations is the fact that the linear theory cannot predict the type of the nonstationary motion, e.g., the motion in the form of a traveling wave or a standing wave. Motivated by premilinary experiments showing roll-like structures, we restrict ourselves to two-dimensional simulations.

A. Description of the method

We have performed nonlinear simulations of nonstationary two-dimensional flows [$v_{my}=0$, ($m=1,2$); the fields of physical variables do not depend on y]. In this case, we can introduce the stream function:

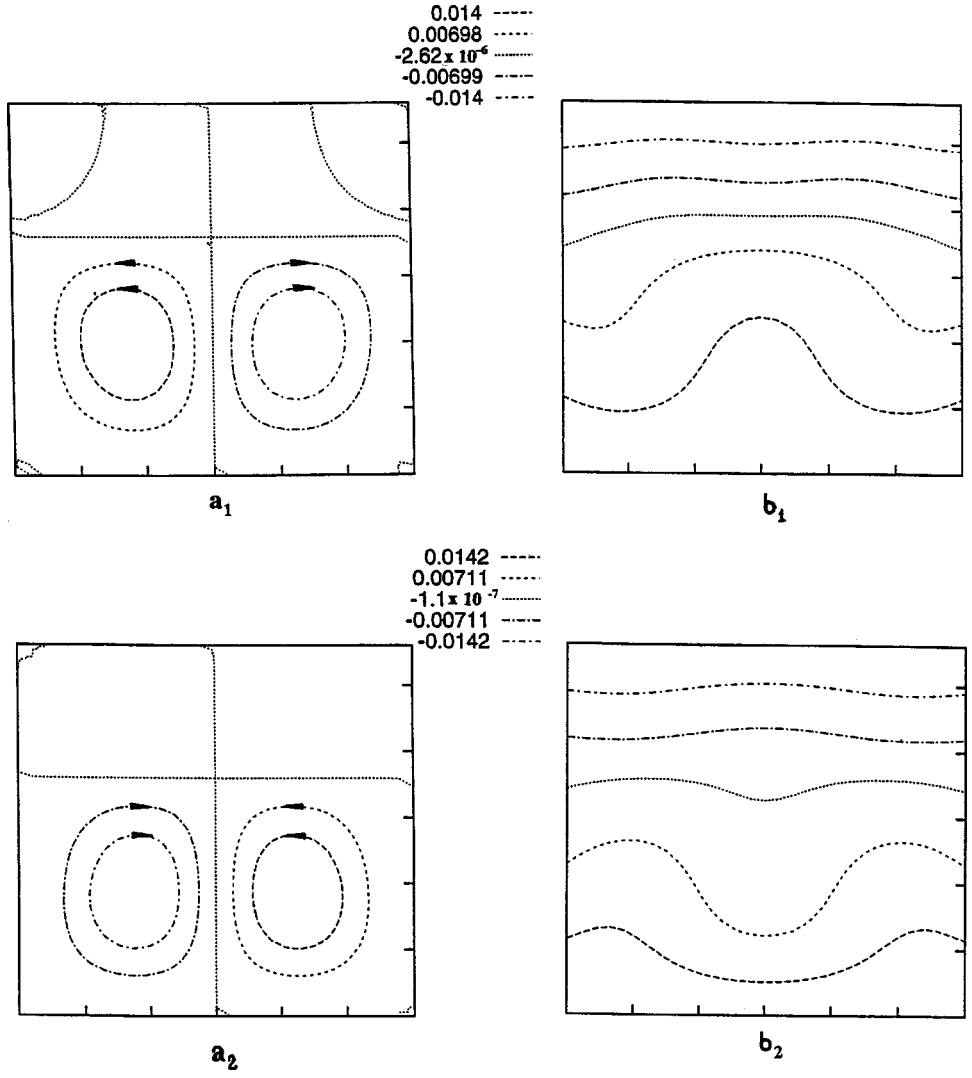

FIG. 9. Stationary convective motions driven by buoyancy. (a) Streamlines and (b) isotherms. The figure shows the two possible solutions named by structure A (a1), (b1) and B (a2), (b2). Parameters: $a=1.8$; $G=18$, $M=0$.

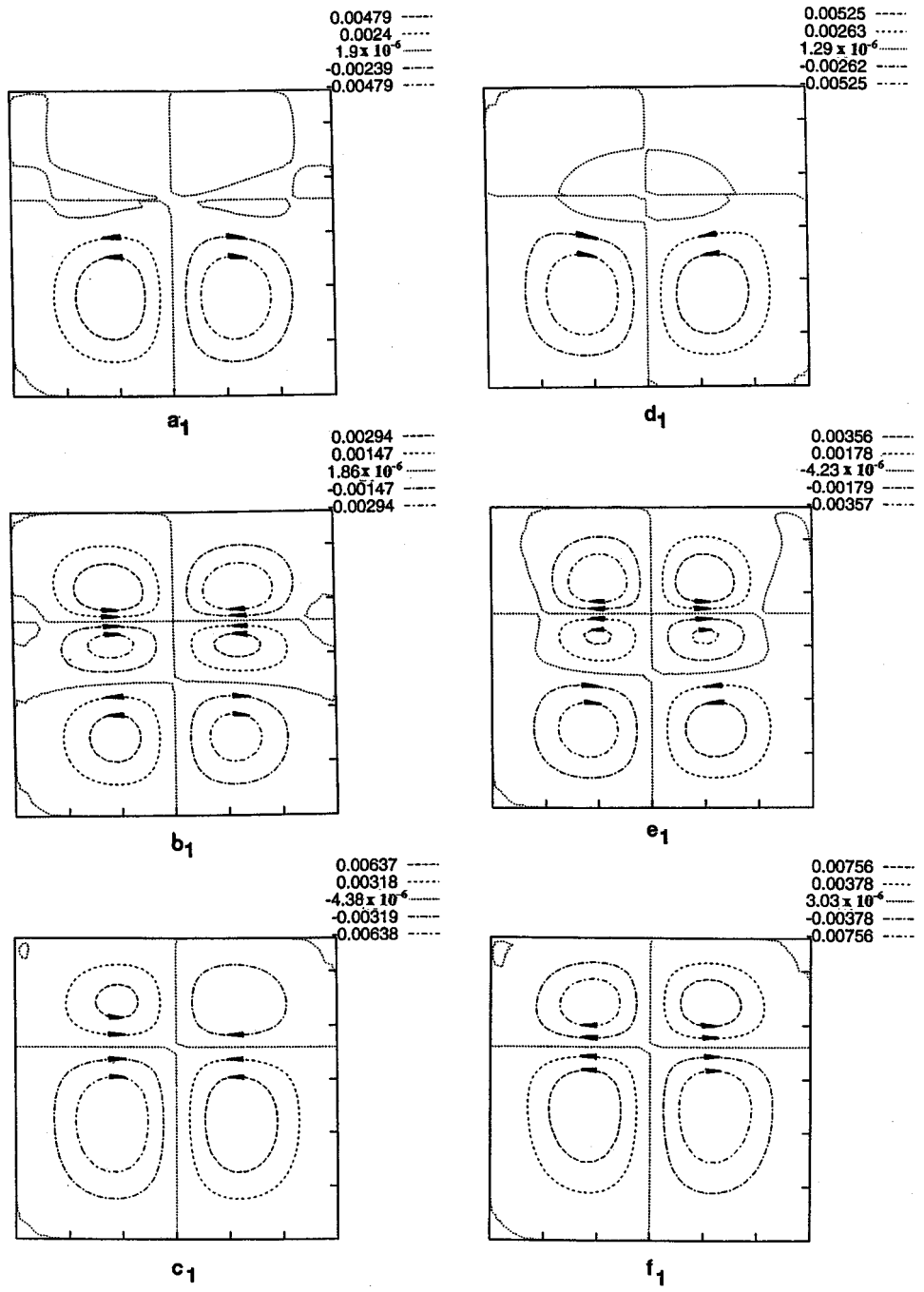

FIG. 10. (a1)–(f1) Streamlines and (a2)–(f2) isotherms for the oscillatory motions in the system with $a=1.8$; $G=18$, $M=-3933$.

$$v_{mx}=\frac{\partial\psi_m}{\partial z},\quad v_{mz}=-\frac{\partial\psi_m}{\partial x}(m=1,2).$$

$$\frac{\partial\phi_m}{\partial t}+\frac{\partial\psi_m}{\partial z}\frac{\partial\phi_m}{\partial x}-\frac{\partial\psi_m}{\partial x}\frac{\partial\phi_m}{\partial z}=c_m\nabla^2\phi_m+b_mG\frac{\partial T_m}{\partial x},\tag{21}$$

Eliminating the pressure and defining the vorticity

$$\phi_m=\frac{\partial v_{mz}}{\partial x}-\frac{\partial v_{mx}}{\partial z},$$

$$\frac{\partial T_m}{\partial t}+\frac{\partial\psi_m}{\partial z}\frac{\partial T_m}{\partial x}-\frac{\partial\psi_m}{\partial x}\frac{\partial T_m}{\partial z}=\frac{d_m}{P}\nabla^2T_m,\tag{22}$$

connected with ψ_m by

$$\nabla^2\psi_m=-\phi_m,\quad m=1,2,\tag{23}$$

$$\nabla^2\psi_m=-\phi_m,$$

we can rewrite the boundary value problem (1)–(9) to the following form:

$$\psi_1=\frac{\partial\psi_1}{\partial z}=0,\quad T_1=0,\quad z=1,\tag{24}$$

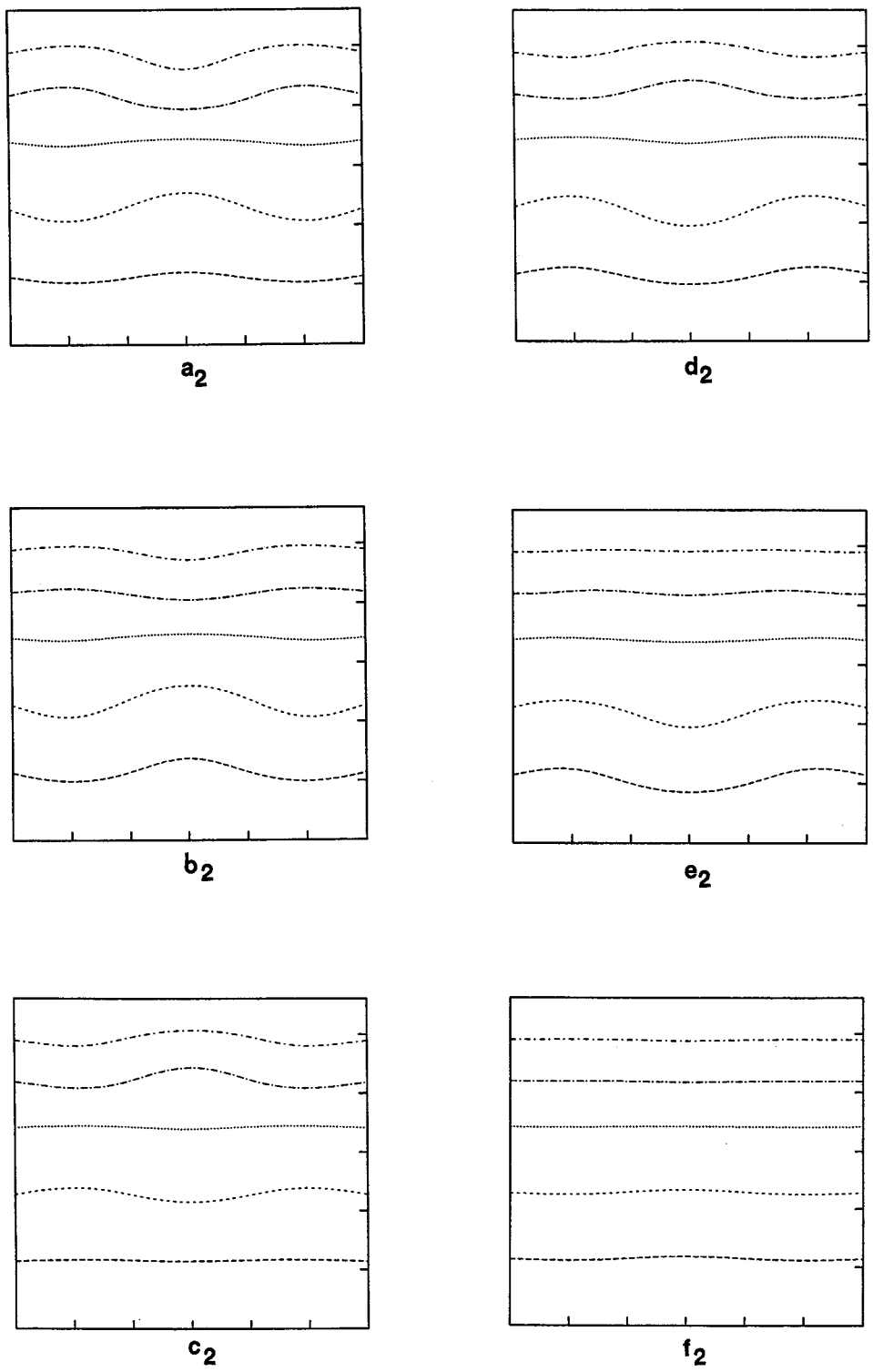

FIG. 10 (*Continued*).

$$\psi_2=\frac{\partial\psi_2}{\partial z}=0, \quad T_2=1, \quad z=-a, \tag{25}$$

$$\psi_1=\psi_2=0, \quad \frac{\partial\psi_1}{\partial z}=\frac{\partial\psi_2}{\partial z}, \quad z=0, \tag{26}$$

$$T_1=T_2, \quad \kappa\frac{\partial T_1}{\partial z}=\frac{\partial T_2}{\partial z}, \tag{27}$$

$$\phi_2=\eta\phi_1+\frac{M\eta}{P}\frac{\partial T_1}{\partial x}. \tag{28}$$

The calculations were performed in a finite region $0<x<L$ with the following types of boundary conditions on the lateral boundaries:

(a) Free heat-insulated boundaries:

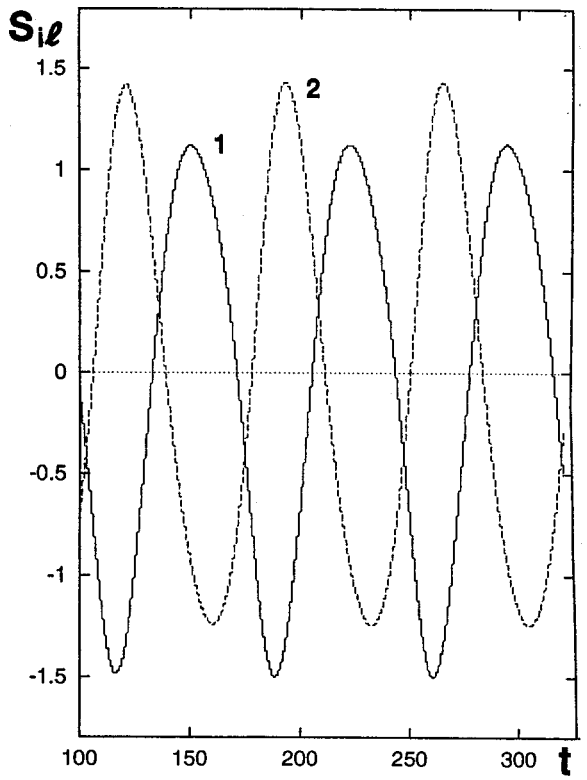

FIG. 11. Time evolution of integral characteristics S_{il}, $i=1,2$; $a=1.8$; $G=18$; $M=-3933$.

$$\psi_m=\phi_m=\frac{\partial T_m}{\partial x}=0, \quad m=1,2, \quad x=0,L. \tag{29}$$

(b) Rigid well-conducting boundaries (with the fixed temperature distribution):

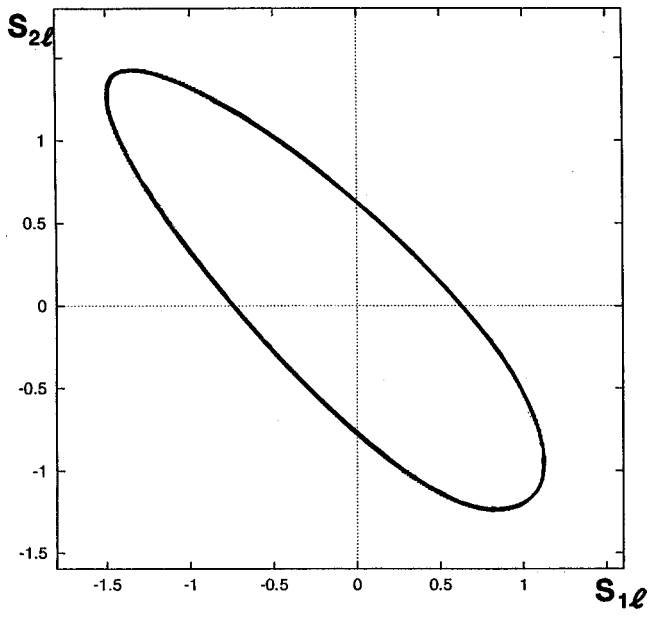

FIG. 12. Phase trajectory of the oscillatory motion; $a=1.8$; $G=18$, $M=-3933$.

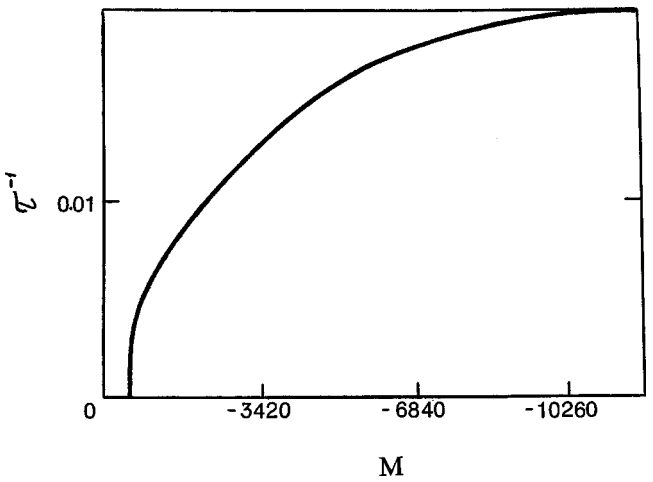

FIG. 13. Dependence of the inverse period of symmetric oscillations τ^{-1} on $-M$.

$$\psi_m=\frac{\partial \psi_m}{\partial x}=0, \quad m=1,2, \quad T_1=\frac{1-z}{1+\kappa a}(z>0),$$

$$T_2=\frac{1-\kappa z}{1+\kappa a} \quad (z<0), \quad x=0,L. \tag{30}$$

The boundary conditions (a) correspond to roll-like spatially periodic patterns in a laterally *infinite* two-layer system, and are used for the comparison of numerical results with those of the linear theory developed for the infinite system. The boundary conditions (b) correspond to a closed cavity with well conducting lateral walls.

The boundary value problem (21)–(30) is solved by the finite difference method (for details, see Ref. [8]). A second order approximation on a uniform mesh is used for the spatial coordinates. The integration of evolution equations is performed by means of an explicit scheme. We used a rectangular mesh 28×56.

In order to estimate the precision of our numerical method, as well as the influence of the lateral boundary conditions on the threshold of the oscillatory instability, we found the critical Grashof number G_* for a fixed value of the Marangoni number $M=-3933$ for geometrical parameters $a=1.8$ and $L=3$. For this goal, we calculated the asymptotic (at large t) growth rate of small disturbances imposed on the equilibrium state. We found $G_*^{(1)}=13.0$ for free heat-insulated boundary conditions (29) and $G_*^{(2)}=17.5$ for rigid isothermic boundary conditions (30). The corresponding critical Grashof number obtained by means of the standard linear theory is $G_*^{(0)}=15.5$. The discrepancy $|(G_*^{(1)}-G_*^{(0)})/G_*^{(0)}|\approx 0.16$ characterizes the precision of our method, while the parameter $|(G_*^{(2)}-G_*^{(1)})/G_*^{(2)}|\approx 0.35$ evaluates the influence of the rigid isothermic boundary conditions.

B. Numerical results

We focus now on the convective motions in the closed cavity having a lateral extension of $L=3$, with well conducting lateral walls. The chosen value of L is close to the wavelength of the critical disturbance. We expect that for such a

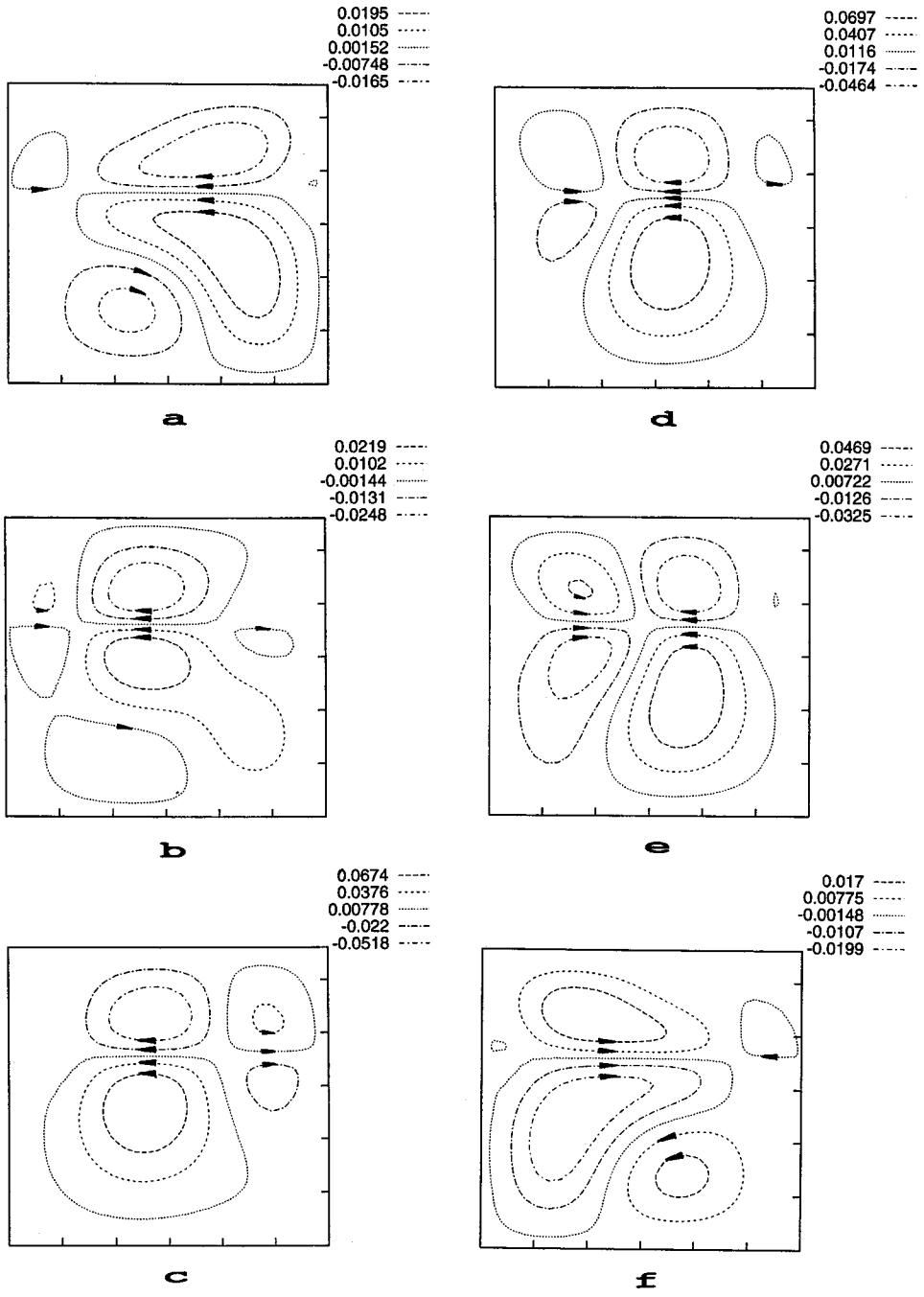

FIG. 14. Streamlines for the asymmetric (type I) oscillatory motion in the system with $a=1.8$, $G=23$, $M=-20\,520$.

value of L the influence of lateral boundaries is essential, but it cannot completely suppress the oscillations.

As was predicted by linear theory, in the case $a=1$ only stationary motions were found. An example of such a motion is shown in Fig. 7. The structure of the motion is typical for the thermocapillary convection in the closed cavity (see Ref. [8]); the buoyancy effects are not essential.

In the case $a=1.8$, both stationary and oscillatory motions were found. The map of regimes is shown in Fig. 8. If the thermocapillary effect is negligible, the convection is stationary, and it takes place mainly in the lower layer (see Fig. 9). There exist two different stable stationary motions with opposite directions of vortices' rotation: structure A with an upward motion in the middle of the lower layer, and structure B with a downward motion in the middle of the lower layer. Both of them are perfectly symmetric:

$$T_m(x,z)=T_m(L-x,z), \quad \psi_m(x,z)=-\psi_m(L-x,z), \quad m=1,2. \tag{31}$$

In the presence of the thermocapillary effect, several types of oscillatory motions can appear. First, let us describe the *symmetric* time-periodic convective oscillations for some fixed values of M and G. In a certain moment of time, the structure of the convective motion [Figs. 10(a1) and 10(a2)] is similar to the structure A of the buoyancy convection (see Fig. 8). The upward motion in the lower layer generates the temperature field on the interface which has a maximum in the middle of the interface. Because of the anomalous ther-

mocapillary effect the tangential stresses appear which are directed toward this maximum. These stresses produce a four-vortex motion near the interface, so that a three-story structure is produced [see Figs. 10(b1) and 10(b2)]. Because the Prandtl numbers of both fluids are rather large, the field of temperature is much more inertial than that of the stream function. That is why the field of temperature generated by the structure A exists during some time and supports both the buoyancy-induced motion in the lower part of the second layer and the thermocapillarity induced motion around the interface. Finally the former motion is completely ousted by the latter one [see Figs. 10(c1) and 10(c2)]. Consequently, the temperature maximum in the middle of the interface disappears. The thermocapillary motion near the interface decays, while in the lower layer the buoyancy convection of the type B is developed [see Figs. 10(d1) and 10(d2)]. The transition between the structures A and B takes place during the first half of the period. The subsequent evolution can be understood in the similar way: the temperature field generated by the structure B produce a thermocapillary motion near the interface [see Figs. 10(e1) and 10(e2)] which replaces the buoyancy-induced motion in the lower layer [see Figs. 10(f1) and 10(f2)], but afterwards the temperature field in the lower layer is rearranged and the structure A [see Figs. 10(a1) and 10(a2)] is restored.

Though the transitions look complicated, actually there are rather simple, weakly nonharmonic oscillations connected with the only oscillatory mode. That becomes clear if we consider the time evolution of integral variables of the motion like

$$S_{1l}(t)=\int_0^{L/2}dx\int_0^1 dz\,\psi_1(x,z,t),$$
$$S_{2l}(t)=\int_0^{L/2}dx\int_{-a}^0 dz\,\psi_2(x,z,t) \tag{32}$$

characterizing the intensity of the motion in the left halves of the layers (see Fig. 11) and the corresponding phase trajectory (see Fig. 12). In every instance of time, the field of the temperature $T(x,z)$ and the field of the stream function $\psi(x,z)$ satisfy the symmetry conditions (31). Therefore the integral variables

$$S_{1r}(t)=\int_{L/2}^{L}dx\int_0^1 dz\,\psi_1(x,z,t),$$
$$S_{2r}(t)=\int_{L/2}^{l}dx\int_{-a}^0 dz\,\psi_2(x,z,t) \tag{33}$$

characterizing the intensity of the motion in the right halves of layers are given by the relations

$$S_{1r}(t)=-S_{1l}(t),\quad S_{2r}(t)=-S_{2l}(t). \tag{34}$$

For a fixed value of G, the frequency of symmetric oscillations grows with $|M|$ (see Fig. 13).

Some different types of oscillations were found for larger values of G. For instance, if the Marangoni number is fixed as $M=-20\,520$, the symmetric oscillations take place in the region $21<G<22.5$. When $G=23$, the symmetric oscillations are unstable, and a certain type (I) of asymmetric time-periodic oscillations appears (see Fig. 14). The latter type of oscillations is characterized by the appearance of vortices of a relatively large horizontal size in the lower (thicker) layer. Note that a similar phenomenon was observed in the case of the steady Rayleigh–Marangoni–Bénard convection in a two-layer system by Cardin and Nataf [33]. The phase trajectory in variables S_{1l}, S_{1r}, which demonstrates the transition between the two types of oscillations is shown in Fig. 15. The symmetry properties (31) and (34) are violated for this type of asymmetric oscillations, but the following relations hold:

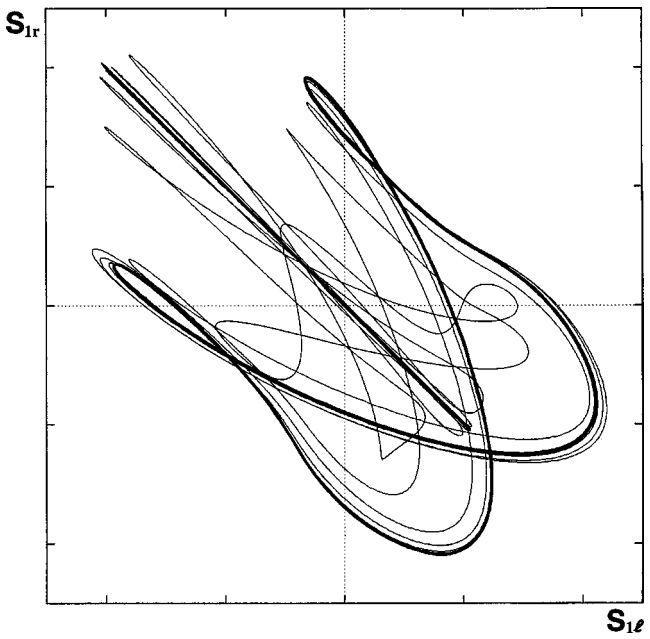

FIG. 15. Transition betweeen symmetric and asymmetric oscillations (type I) on the phase plane (S_{1l},S_{1r}); $G=23$, $M=-20\,520$.

$$T_m(x,z,t+\tau/2)=T_m(L-x,z,t),$$
$$\psi_m(x,z,t+\tau/2)=-\psi_m(L-x,z,t),\quad m=1,2, \tag{35}$$

where τ is the period of oscillations. Therefore, the phase trajectory in variables S_{1l}, S_{1r} is symmetric [see Fig. 16(a)].

If the absolute value of the Marangoni number $|M|$ decreases for a fixed $G=28$, a transition from the asymmetric oscillations of the type I to another type (II) of asymmetric time-periodic oscillations takes place. The phase trajectory in variables S_{1l}, S_{1r} is not symmetric anymore [see Figs. 16(b) and 16(c)]; thus, (35) does not hold. Actually, there are two different solutions connected by the transformation $x\to L-x$. We note that there is a wide hysteresis between asymmetric oscillations and symmetric stationary motions. For lower values of $|M|$ complicated time periodic [see Figs. 16(d) and 16(e)] and aperiodic oscillatory motions take place. At $G=31$ the asymmetric oscillations of the type I are restored [see Fig. 16(f)].

We have also calculated convective motions in cavities with larger values of the aspect ratio L. We came to the conclusion that the oscillatory structures are qualitatively similar to those found at $L=3$. A snapshot of an oscillatory

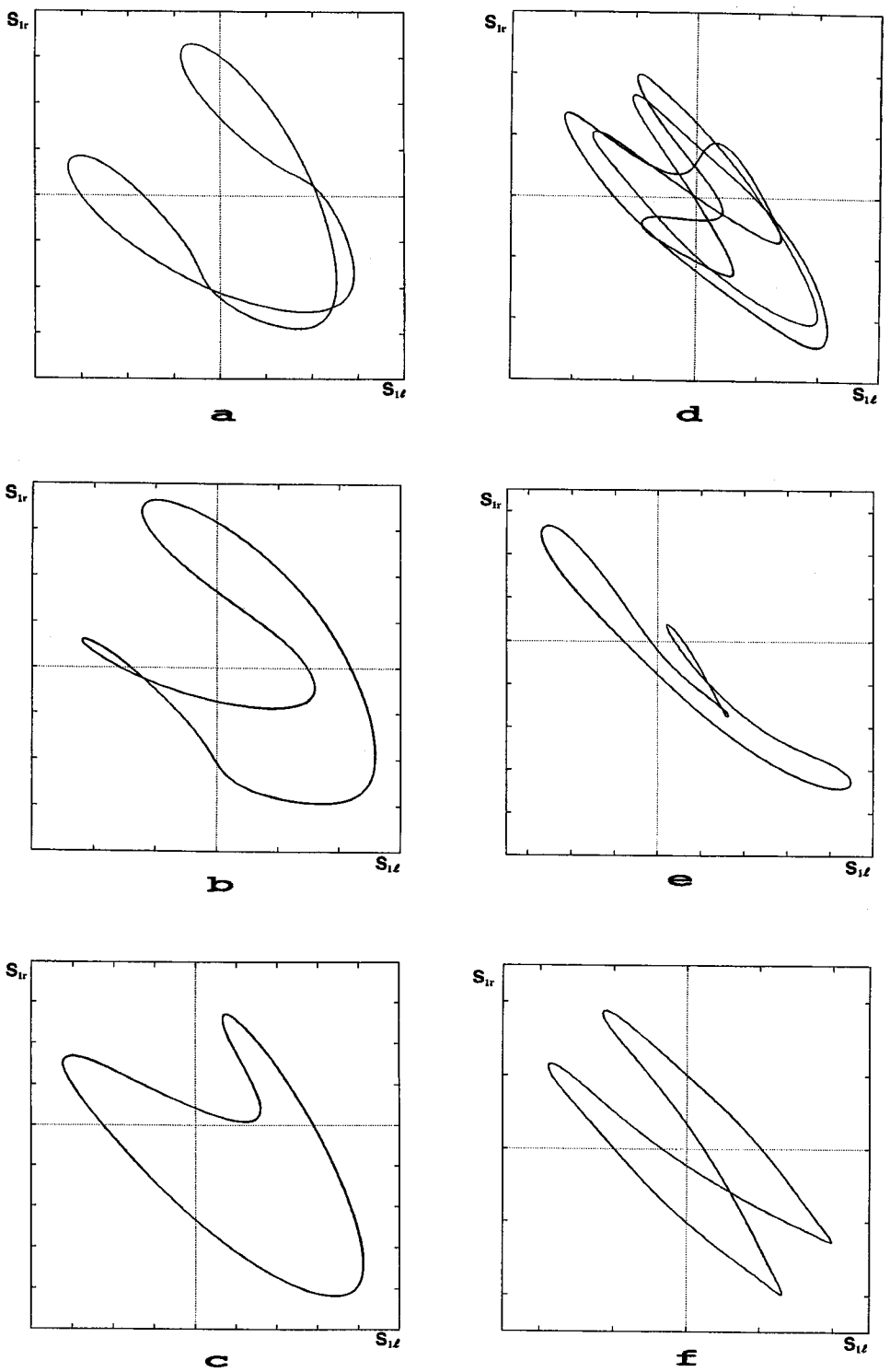

FIG. 16. Phase trajectories: (a) $G=28$, $M=-20\,520$; (b) $G=28$, $M=-11115$; (c) $G=28$, $M=-3078$; (d) $G=28$, $M=-2394$; (e) $G=28$, $M=-770$; (f) $G=31$; $M=-2394$.

motion at $L=6$ is shown in Fig. 17. As was mentioned above, in the lower (thicker) layer one observes some vortices of a relatively large horizontal size (see Ref. [33]).

V. CONCLUSIONS

We found that the combined action of the buoyancy and the anomalous thermocapillary effect generates some specific new types of convective oscillations. The nature of the considered oscillatory instability mechanism is different from both Rayleigh–Bénard oscillations and Marangoni oscillations. The appearance of the previously oscillations is caused by the *competition* of the buoyancy and the anomalous thermocapillary effect. The observed oscillations have different symmetry properties. The stability regions of oscillations and stationary motions overlap.

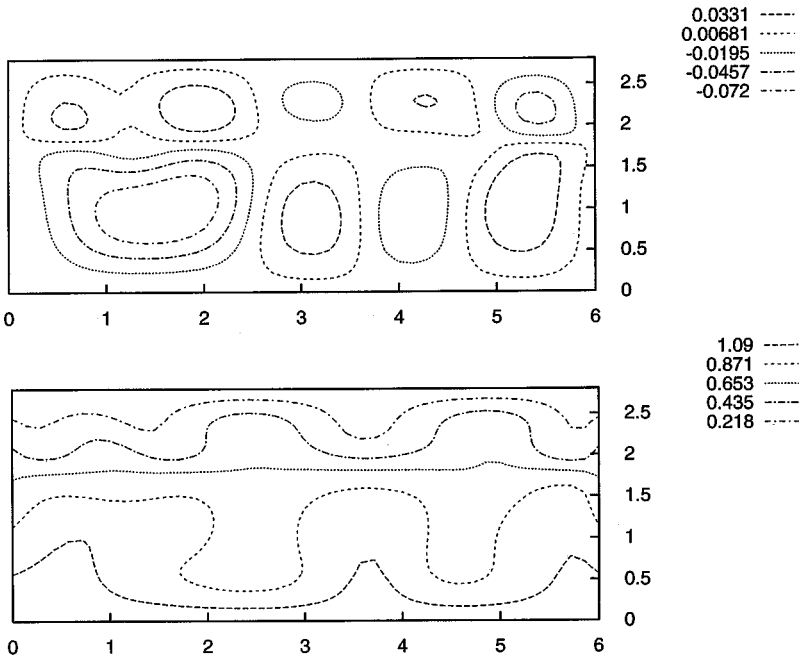

FIG. 17. (a) Streamlines and (b) isotherms for the oscillatory motion in the system with $L=6$ ($G=40$, $M=-6849$).

ACKNOWLEDGMENTS

This work was supported in part by the German–Israeli Foundation for Scientific Research and Development and by the Fund for the Promotion of the Research at Technion. I.B.S. acknowledges the support of the Israeli Ministry of Science and Humanities and the Ministry of Absorption. I.B.S. is grateful to D. Kessler and L. Shtilman for their help and encouragement. A.A.N. is indebted to P. Colinet for fruitful advice. We thank André Holzhey for his help.

[1] F. H. Busse, Rep. Prog. Phys. **41**, 1929 (1978).
[2] M. C. Cross and P. C. Hohenberg, Rev. Mod. Phys. **65**, 851 (1993).
[3] I. B. Simanovskii, Fluid Dyn. **14**, 637 (1979).
[4] G. Z. Gershuni and E. M. Zhukhovitsky, Dokl. Acad. Nauk SSSR **265**, 302 (1982) [Sov. Phys. Dokl. **27**, 531 (1982)].
[5] A. Yu. Gilev, A. A. Nepomnyashchy, and I. B. Simanovskii, in *Viscous Fluid Dynamics*, edited by V. A. Briskman, B. I. Myznikova, and E. V. Slavnov (USC AS USSR, Sverdlovsk, 1987), pp. 36 and 37 (in Russian).
[6] S. Rasenat, F. H. Busse, and I. Rehberg, J. Fluid Mech. **199**, 519 (1989).
[7] P. Colinet and J.-C. Legros, Phys. Fluids **6**, 2631 (1994).
[8] I. B. Simanovskii and A. A. Nepomnyashchy, *Convective Instabilities in Systems with Interface* (Gordon and Breach Science, London, 1993).
[9] E. L. Koschmieder, *Bénard Cells and Taylor Vortices* (Cambridge University Press, London, 1993).
[10] M. Bestehorn, Phys. Rev. E **48**, 3622 (1993).
[11] A. Thess and M. Bestehorn, Phys. Rev. E **52**, 6358 (1995).
[12] K. Eckert, M. Bestehorn, and A. Thess, J. Fluid Mech. **356**, 155 (1998).
[13] A. A. Golovin, A. A. Nepomnyashchy, and L. M. Pismen, J. Fluid Mech. **341**, 317 (1997).
[14] K. A. Smith, J. Fluid Mech. **24**, 401 (1966).
[15] S. J. Van-Hook, M. F. Schatz, W. D. McCormick, J. B. Swift, and H. Swinney, J. Fluid Mech. **345**, 45 (1997).
[16] C. V. Sternling and L. E. Scriven, AIChE J. **5**, 514 (1959).
[17] J. R. Reichenbach and H. Linde, J. Colloid Interface Sci. **81**, 433 (1981).
[18] A. A. Nepomnyashchy and I. B. Simanovskii, Fluid Dyn. **18**, 629 (1983).
[19] A. A. Nepomnyashchy and I. B. Simanovskii, Dokl. Acad. Nauk SSSR **272**, 825 (1983) [Sov. Phys. Dokl. **28**, 838 (1983)].
[20] E. B. Levchenko and A. L. Chernyakov, Zh. Eksp. Teor. Fiz. **81**, 202 (1981) [Sov. Phys. JETP **54**, 102 (1981)].
[21] P. L. Garcia-Ybarra and M. G. Velarde, Phys. Fluids **30**, 1649 (1987).
[22] D. A. Nield, J. Fluid Mech. **19**, 341 (1964).
[23] R. W. Zeren and W. C. Reynolds, J. Fluid Mech. **53**, 305 (1972).
[24] E. N. Ferm and D. J. Wollkind, J. Non-Equilib. Thermodyn. **7**, 170 (1982).
[25] A. A. Nepomnyashchy and I. B. Simanovskii, Fluid Dyn. **19**, 494 (1984).
[26] P. M. Parmentier, V. C. Regnier, and G. Lebon, Phys. Rev. E **54**, 411 (1996).
[27] P. Cerisier, C. Jamond, J. Pantaloni, and C. Perez-Garcia, Phys. Fluids **30**, 954 (1987).
[28] W. A. Tokaruk, T. C. A. Molteno, and W. Morris, Phys. Rev. Lett. **84**, 3590 (2000).
[29] A. Yu. Gilev, A. A. Nepomnyashchy, and I. B. Simanovskii, Fluid Dyn. **22**, 142 (1987).
[30] J. C. Legros, Acta Astron. **13**, 697 (1986).
[31] K. Eckert and A. Thess (unpublished).
[32] H. C. Nataf, S. Moreno, and Ph. Cardin, J. Phys. (France) **49**, 1707 (1988).
[33] P. Cardin and H.-C. Nataf, Europhys. Lett. **14**, 655 (1991).
[34] Ph. Cardin, H.-C. Nataf, and Ph. Dewost, J. Phys. II **1**, 599 (1991).